Two-dimensional numerical modeling of wood transport

Virginia Ruiz-Villanueva, Ernest Bladé, Martí Sánchez-Juny, Belén Marti-Cardona, Andrés Díez-Herrero and José María Bodoque

ABSTRACT

The transport of wood material in rivers has been the subject of various studies in recent years. Most research has focused on the ecological and geomorphologic role of wood, its recruitment processes and spatial distribution in streams. In this study, we focused on wood transport dynamics, and we have developed a numerical model to simulate wood transport coupled with a two-dimensional (2D) hydrodynamic model. For this purpose, wood drag forces were incorporated as additional source terms into the shallow water equations, which are solved together with wood transport by using the finite volume method. This new tool has been implemented as a computational module into 'Iber', a 2D hydraulic simulation software. The new module analyzes the initial motion threshold of wood based on the balance of forces involved in the wood's movement, and computes the position and velocity of differently shaped logs using a kinematic approach. The method also considers the interaction between the logs themselves and between the logs and the channel walls or boundaries. Flume experiments were used in a straight channel with obstructions to validate the model's capacity to accurately reproduce the movement of floating logs.

Key words | 2D hydraulic modeling, flume, 'Iber' 2D model, large wood, river flow, woody debris

Virginia Ruiz-Villanueva (corresponding author)
Andrés Díez-Herrero
Department of Research and Geoscientific Prospective,
Geological Survey of Spain,
Instituto Geológico Minero de España (IGME),
Ríos Rosas 23, E-28003 Madrid,
Spain
E-mail: *virginiaruizv@gmail.com*; *virginia.ruiz@dendrolab.ch*

Ernest Bladé
Martí Sánchez-Juny
Belén Marti-Cardona
Flumen Research Institute,
Universitat Politècnica de Catalunya – Barcelona Tech,
Jordi Girona 1-3, (D1), E-08034, Barcelona,
Spain

José María Bodoque
Facultad de Ciencias Ambientales y Bioquímica,
Universidad de Castilla – La Mancha,
Avda. Carlos III s/n, E-45071 Toledo,
Spain

NOTATION

A'	Projection of cross-area of the log in the flow direction
A_i	Area of mesh element i
A_{sub}	Submerged area of the log perpendicular to piece length
A_w	Area of the log perpendicular to the piece length
C^*	Transport inhibition parameter
C_{d}	Drag coefficient
D_w	Log diameter
e	Restitution coefficient
F_d	Drag force
$\mathbf{F}_d$	Drag force (vector)
F_f	Friction force opposite to the flow direction
F_g	Gravitational force in the downstream direction
F_n	Normal force
F_w	Effective weight of log
g	Gravity
h	Water depth
L_w	Log length
L_w^{wet}	Length of the log inside the river channel
m_i	Mass of log i
U	Water velocity
U_{lim}	Threshold velocity
U_{log}	Component of log velocity in the direction of the flow
$\mathbf{v}$	Water velocity (vector)
$\mathbf{v}^{1,2}$	Water velocity at log ends (vector)
$\mathbf{v}^{cm}$	Water velocity of the log center (vector)
$(\mathbf{v}_{\text{log}})^{cm}$	Velocity of the mass center of two colliding logs (vector)
$(\mathbf{v}_{\text{log}})^{i}$	Velocity of log i (vector)
$(\mathbf{v}'_{\text{log}})^{i}$	Final velocity of log i (vector)
$\mathbf{x}^{1,2}$	Position of log ends (vector)
$\mathbf{x}'^{1,2}$	Final position of log ends (vector)
$\mathbf{x}^{cm}$	Log center position (vector)
$\mathbf{x}'^{cm}$	Final log center position (vector)

doi: 10.2166/hydro.2014.026

α	Angle of the channel bed in the direction of the flow
Δt	Time step
ρ	Water density
ρ_w	Wood density
μ_{bed}	Friction coefficient between the wood and the river bed
θ	Angle of the log relative to flow
θ'	Final log orientation
$\tau_{\text{wood}i}$	Shear stress due to log presence
σ_s	Angle between log and wall

INTRODUCTION

Large wood (LW) forms an important component of river ecosystems (Gurnell *et al.* 2002; Collins *et al.* 2012). These woody pieces interact with flow to create complex channel features, which triggers morphological and hydraulic changes (Montgomery 2003). LW also provides essential habitats for fishes and riverine species (Jackson & Sturm 2002; Langford *et al.* 2012 and references within) and enhances riparian forest regeneration (Abbe & Montgomery 2003).

In spite of these important consequences of wood in fluvial corridors on stream hydraulics, morphology and sediment transport, its dynamics and effects were barely considered by researchers until the 1980s, and to date knowledge of woody material transport processes is still limited. Most studies have focused on the morphological role of LW (Montgomery & Piégay 2003; Swanson 2003; Moulin & Piégay 2004), using vegetation as a tool in the interpretation of fluvial geomorphic processes (Hupp & Bornette 2003; Seo & Nakamura 2009). Other studies analyzed its recruitment processes (Martin & Benda 2001; Benda & Sias 2003; May & Gresswell 2003; Webb & Erskine 2003; Kasprak *et al.* 2011) and its spatial distribution in mountain streams (Jackson & Sturm 2002; Comiti *et al.* 2006, 2008a, 2008b, 2012; Andreoli *et al.* 2007; Wohl & Jaeger 2009; Wohl 2011; Wohl *et al.* 2011), low-gradient rivers (Magilligan *et al.* 2008; Curran 2010; Moulin *et al.* 2011) and modified rivers or urbanized areas (Thevenet *et al.* 1998; Lassettre & Kondolf 2012).

From a hydraulic perspective, the influence of LW on flow resistance has only been examined by a few researchers (Manga & Kirchner 2000; MacFarlane & Wohl 2003; Wilcox *et al.* 2008; Allen & Smith 2012). Some studies have attempted to characterize the transport and hydrodynamics of wood in rivers in quantitative terms. In this regard, LW mobilization has been investigated in laboratory flumes either by combining detailed hydraulic predictions of flume studies with real data from field studies, and/or through analytical approaches. The first works carried out by Braudrick & Grant (2000) and Braudrick *et al.* (2001) provided the basic framework to approach wood mobility. Following this, some other works were carried out to explore dynamics of wood in rivers, i.e. Haga *et al.* (2002), Bocchiola *et al.* (2002, 2006). These studies successfully predicted woody material entrainment based on the balance of hydrodynamic and resistance forces and some of them dealt with transport regimes. Some have used these approaches to describe the mobility of wood in streams (Manners *et al.* 2007; Curran 2010), while other experimental attempts focused on the influence of LW on sediment transport and deposit (Wallerstein *et al.* 2001). However, since LW tends to move during large floods, there are little direct observations and measurements of wood transport. Thus, in recent years, a few studies have been carried out to develop precise monitoring techniques for tracking and quantifying the temporal dynamics of wood, demonstrating the relationship between wood and discharge and the fact that wood transport is more complicated than previously theorized on the basis of flume-scale experiments (MacVicar *et al.* 2009; MacVicar & Piégay 2012).

However, as pointed out by some researchers (see Braudrick & Grant 2000; Mazzorana *et al.* 2011b, among others), to date no deterministic hydrodynamic model has been able to simulate the transport of multiple LW elements of different sizes under complex hydraulic conditions at relatively short timescales.

Therefore, the main aim of this work is to develop a numerical method for simulating the transport of wood together with hydrodynamics. This paper shows the new developed numerical module in detail, the governing equations, variables, parameters and coefficients, and its validation by means of flume experiments.

The paper is divided into seven main sections: the first two sections are the general introduction and the description of the two-dimensional (2D) hydraulic model 'Iber'; followed by the model set-up; the experimental study and observation methods; the validation of the model and compares experimental and numerical results. The penultimate section discusses the results obtained, highlighting the implications and limitations of the proposed numerical model at present. In addition, a discussion of potential applications and use in real rivers are also provided, followed by the conclusions.

DESCRIPTION OF THE NUMERICAL MODEL

The method presented here was coupled as a new module to 'Iber' (Corestein *et al.* 2010; Bladé *et al.* 2012), a two-dimensional hydrodynamic software developed by the International Center of Numerical Methods in Engineering (CIMNE), the Water and Environment Engineering Group (GEAMA) (UDC) and the Flumen Research Institute (Universitat Politècnica de Catalunya (UPC)). 'Iber' (www.Iberaula.es) is a numerical analysis 2D tool for computations of turbulent free surface unsteady flow and sediment transport in watercourses. At present, 'Iber' has three main computational modules: a hydrodynamic module, a turbulence module and a sediment transport module. The hydrodynamic module solves depth-averaged shallow water equations (2D-SWE or two-dimensional Saint Venant equations). The turbulence module allows turbulent stresses to be included in the hydrodynamic computations, and includes different turbulence models based on the Bousineq turbulent viscosity approximation (a parabolic model, a mixing length model, and a k–ε model). The sediment transport module solves the Exner sediment conservation equation together with the bedload and the suspended load transport equations to predict the evolution of the riverbed.

In 'Iber', the hydrodynamics, turbulence and sediment transport are solved using the finite volume method (FVM) with a high resolution (second order and non-oscillatory) extension of Roe's upwind scheme, a time explicit scheme, on non-structured meshes. The FVM is widely used in computational fluid dynamics (Leveque 2002; Versteeg & Malalasekera 2007), and has also been used for shallow water equations since the late-1990s, when Vázquez-Cendón (1999) managed to develop a well-balanced scheme. Recently, the method has also been implemented in commercial software packages for flood analysis, such as Infoworks (Gutierrez-Andres *et al.* 2008), the latest versions of Mike Flood (DHI 2007) and Tuflow, or Guad2D (Murillo *et al.* 2008), mainly because of its advantages when simulating flows with shocks, such as front waves or hydraulic jumps, and the possibility of using unstructured irregular meshes.

The wood transport module presented here allows the inclusion of wood pieces in the simulations by means of a Langrangian discretization. The method couples the flow variables calculated with the hydrodynamic module to update the position and velocity of the wood logs at every time step. Therefore, wood transport method presented here could be combined with any other 2D explicit numerical scheme based on the finite volume or the finite element methods (FVM and FEM, respectively).

In order to incorporate wood transport into the model, wood and boundary conditions are first established. Therefore, flow conditions exert an influence on the logs but there is also an opposite effect, as the presence of logs will affect the flow.

The main simplification assumed by the model is the shape of the logs as cylinders, avoiding variations in shape (variations in diameter) and the effect of branches or roots. This geometry may be not representative of LW with complex shapes (Allen & Smith 2012), but it provides a good approximation of non-rooted and defoliated logs often occurring in rivers as a result of fluvial transport, wood harvesting and forest fires (see Braudrick *et al.* 1997; Bocchiola *et al.* 2008; Buxton 2010; Bocchiola 2011; Mazzorana *et al.* 2011a). If branches or roots are present on the logs, then the presented model may fail with regard to the log movement simulation.

Braudrick & Grant (2000) proposed a theoretical method to attach the rootwad to a log using a disk on the cylinder ends. The authors expect to overcome this limitation in future developments.

Log incipient motion and velocity

In order to determine wood entrainment, our model governing equation is based on the Lagrangian formulation proposed by Braudrick & Grant (2000) and Haga *et al.* (2002), used

here in a two-dimensional space. This governing equation is the balance of forces in the direction of flow acting on a piece of wood situated in the water stream (Figure 1(a)). Log velocity, considered as a two-dimensional vector in the horizontal plane, is calculated for each time step.

The gravitational force (F_g) acting on the log is equal to the effective weight of the log (F_w) in the downstream direction, and is equal to:

$$F_g = F_w \cdot \sin\alpha = (g \cdot \rho_w \cdot L_w \cdot A_w - g \cdot \rho \cdot L_w \cdot A_{\text{sub}}) \cdot \sin\alpha \tag{1}$$

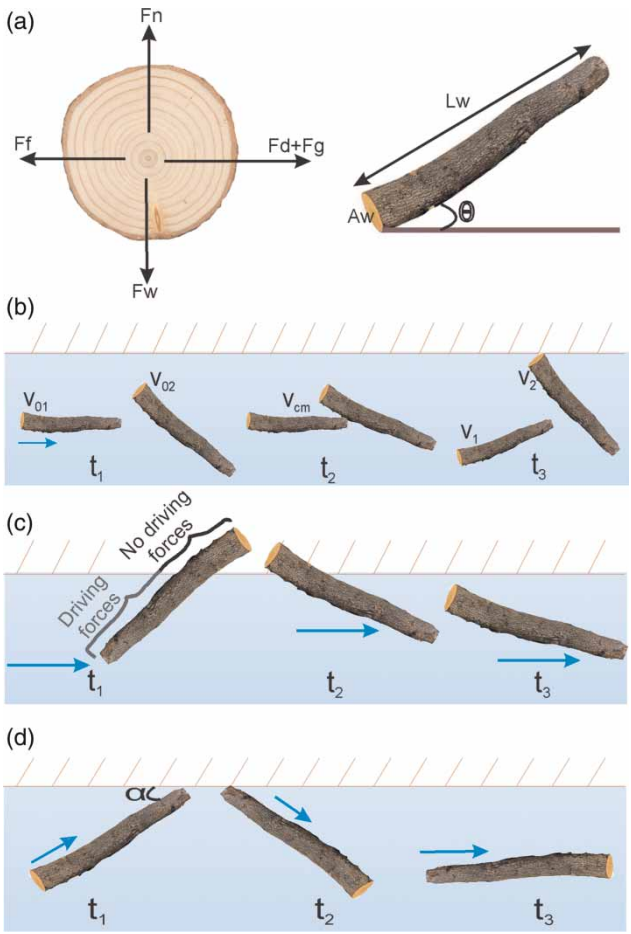

Figure 1 | (a) Schematic and body-force diagram of the force balance components acting on a cylindrical piece of wood. (b) One piece of wood is moving in the flow direction and meets another piece; they collide and after the collision they continue moving at different velocities. (c) Part of the log is out of the river (dry area) then driving forces are re-calculated. (d) Log hits the bank (wall) and slides or bounces off depending on the incidence angle α. Different time steps are represented as t_1, t_2 and t_3.

where L_w is the piece length, ρ_w and ρ are the wood and water densities, respectively, α is the angle of the channel bed in the direction of the flow, g is gravity, A_w is the area of the log perpendicular to the piece length:

$$A_w = \pi \cdot D_w^2/4 \tag{2}$$

and A_{sub} is the submerged area of the log perpendicular to piece length. A_{sub} is a function of the log draft (y) and piece diameter (D_w), which for a right-circular cylinder resolves to:

$$A_{\text{sub}} = [2 \cdot \cos^{-1}(1 - 2 \cdot y/D_w) - \sin(2 \cdot \cos^{-1}(1 - 2 \cdot y/D_w))] \cdot D_w^2/8 \tag{3}$$

and the projected log area:

$$A' = A_{\text{sub}} \cdot \cos\theta + y \cdot L_w \cdot \sin\theta \tag{4}$$

where θ is the angle of the piece relative to flow, with $\theta = 0^\circ$ when the log is parallel to flow, and h is the flow depth.

The friction force (F_f) acting in the contrary direction to the flow is equal to the normal force $(F_n = F_w \cdot \cos\alpha)$ acting on the log times, the coefficient of friction between the wood and the bed:

$$F_f = F_n \cdot \mu_{\text{bed}} = (g \cdot \rho_w \cdot L_w \cdot A_w - g \cdot \rho \cdot L_w \cdot A_{\text{sub}}) \cdot \mu_{\text{bed}} \cdot \cos\alpha \tag{5}$$

where μ_{bed} is the coefficient of friction between the wood and the bed.

The drag force (F_d), also in the flow direction, is the downstream drag exerted on the log and is equal to:

$$F_d = -(U - U_{\log})^2/2 \cdot \rho \cdot C_d \cdot (L_w \cdot y \cdot \sin\theta + A_{\text{sub}} \cdot \cos\theta) \tag{6}$$

where U is the water velocity, $U_{\log}$ is the component of the log velocity in the direction of the flow and C_{d} is the drag coefficient of the wood in water. C_{d} is an important parameter in log velocity computations. Natural pieces of wood may have a greater drag due to skin friction (Merten *et al.* 2010), but this has not been taken into account in

this paper. This coefficient also varies with the log shape, its position in the stream and Reynolds number. In this work, a constant value is used for the drag coefficient, although this can be modified for each log if desired. Drag coefficients values for many different shapes of bodies have been studied extensively. Brooks *et al*. (2006) reviewed the literature and selected a value of 1.2 for wood in streams, whereas Bocchiola *et al*. (2006) used 1.41 for dowels in a flume. We have taken the value proposed by this latter author.

The combination of the last three equations yields the force balance at incipient motion for a circular cylinder lying on the river bed: $F_f = F_g + F_d$

$$\begin{aligned}&(g \cdot \rho_w \cdot L_w \cdot A_w - g \cdot \rho \cdot L_w \cdot A_{\text{sub}}) \cdot (\mu_{\text{bed}} \cdot \cos\alpha - \sin\alpha) \\ &= U^2/2 \cdot \rho \cdot C_d \cdot (L_w \cdot h \cdot \sin\theta + A_{\text{sub}} \cdot \cos\theta)\end{aligned} \tag{7}$$

where h is the water depth. Thus, the velocity corresponding to $(F_g + F_d)/F_f = 1$, here called threshold velocity U_{lim}, for the movement of the wood element (the incipient motion), is determined by:

$$U_{\text{lim}}^2 = \frac{((g \cdot \rho_w \cdot L_w \cdot A_w) - (g \cdot \rho \cdot A_{\text{sub}} \cdot L_w)) \cdot (\mu_{\text{bed}} \cdot \cos\alpha - \sin\alpha)}{(0.5 \cdot C_d \cdot \rho \cdot (L_w \cdot h \cdot \sin\theta + A_{\text{sub}} \cdot \cos\theta))} \tag{8}$$

We followed the nomenclature proposed by Mazzorana *et al.* (2011a), with some modifications. These authors used the average flow velocity (U) as the reference velocity for the moving woody material for a wide range of flow conditions. Then the velocity for a moving log (U_{log}) is

$$U_{\text{log}} = (1 - C^*) \cdot U \tag{9}$$

where C^* is a transport inhibition parameter, which is equal to 0 when the wood material element is floating, C^* is equal to 1 when a resting condition is imposed on the wood material, and $C^* = 1 - h/D_w$ if the transport regime is either sliding or rolling.

Since the developed numerical model calculates the flow and log velocities at every time step, we modified the transport inhibition parameter (C^*) proposed by Mazzorana *et al*. (2011a) using the relative velocity of the water in relation to the log velocity, instead of the average flow velocity ($U_r = U - U_{\text{log}}$) as

$$C^* = U_{\text{lim}}/U \tag{10}$$

Then, substituting C^* in Equation (9)

$$U_{\text{log}} = U - U_{\text{lim}} \tag{11}$$

Given these results and based on log density, log diameter and water depth, four main scenarios can be distinguished and related to the transport regimes: (i) scenario A, the log density is assumed to be greater than the water density, and the water depth is lower than the log diameter and equal to the submerged log diameter. In this situation, if $U_{\text{lim}} \geq U$ the resting condition is imposed on the log, and if $U_{\text{lim}} < U$ the log will move, sliding with velocity $U_{\text{log}} = U - U_{\text{lim}}$; (ii) scenario B: when the log density is greater than the water density and the water depth is higher than the log diameter and higher than the submerged log diameter, i.e. the log is completely submerged, then again if $U_{\text{lim}} < U$ the log will move and slide, otherwise it will not. The velocity for a moving log is $U_{\text{log}} = U - U_{\text{lim}}$where now

$$U_{\text{lim}}^2 = \frac{(\rho_w - \rho) \cdot g \cdot L_w \cdot A_w \cdot (\mu_{\text{bed}} \cdot \cos\alpha - \sin\alpha)}{0.5 \cdot C_d \cdot \rho \cdot (L_w \cdot D_w \cdot \sin\theta + A_w \cdot \cos\theta)} \tag{12}$$

(iii) scenario C: when the log density is equal to or lower than the flow density and the water depth is higher than the log diameter and higher than the submerged log diameter, then the log will float ($U_{\text{lim}} = 0$ and $U_{\text{log}} = U$) and will be transported with a velocity equal to the flow velocity, except in the case of interaction with other logs or channel walls; (iv) scenario D, the log density is equal to or lower than the flow density and the water depth is lower than the log diameter and equal to the submerged log diameter, then U_{lim} is calculated in the same way as in scenario A.

As well as sliding, a piece may also move by rolling (Bocchiola *et al.* 2006) in scenarios A, B and D, but the movement forces involved in this case are beyond the scope of this study. Here the focus was on validating the floating regime, since dry wood generally has a specific gravity less than water and therefore readily floats (Montgomery 2003). However, the model is able to simulate the transport

of a submerged or saturated log through sliding transport regime using Equations (11) and (12). In any case, once the log velocity in the flow direction $U_{\log}$ has been calculated, the log position, or position of the log center $\mathbf{x}^{cm} = (x_1^{cm}, x_2^{cm})$ is updated at every time step to its final position $\mathbf{x}'^{cm}$

$$\mathbf{x}'^{cm} = \mathbf{x}^{cm} + \Delta t \cdot \mathbf{v}^{cm} \tag{13}$$

$\mathbf{v}^{cm} = (v_1^{cm}, v_2^{cm})$ is the velocity of the log center, which is in the direction of the flow but of value $U_{\log}$

$$\mathbf{v}^{cm} = U_{\log} \cdot \mathbf{v}/|\mathbf{v}| \tag{14}$$

Apart from the translatory movement described, logs turn driven by the velocity distribution across the flow section. If one end of the piece of wood is moving faster than the other, the piece rotates towards a more flow-parallel orientation. Since the velocity field still varies across the piece, the piece continues to rotate towards a flow-parallel orientation until it reaches a stable orientation. To simulate these changes in orientation, the velocities at each end of every log are obtained from the flow model. Depending on the mesh size with respect to the log size, one log can be contained in a single mesh element (finite volume) or in more than one. The flow velocity at each end (1 or 2) of the log $\mathbf{v}^{1,2} = (v_1, v_2)^{1,2}$ is calculated from the flow velocity at the log center $\mathbf{v}$, the flow velocity gradients and the relative position of the log ends $\mathbf{x}^{1,2} = \left(x_1^{1,2}, x_2^{1,2}\right)$ with respect to the log center position $\mathbf{x}$

$$v_i^{1,2} = v_i + \frac{\partial v_i}{\partial x_j} \cdot \left(x_j^{1,2} - x_j\right) \tag{15}$$

From the velocity values at the log ends, it is possible to obtain the new value of log orientation at every time step

$$\theta' = \tan^{-1}\left(\frac{x_2'^2 - x_2'^1}{x_1'^2 - x_1'^1}\right) \tag{16}$$

where:

$$\mathbf{x}'^{1,2} = \mathbf{x}^{1,2} + \Delta t \cdot \mathbf{v}^{1,2} \tag{17}$$

Effect of wood transport on water flow

The influence of wood on hydrodynamics has been well described, e.g. as Gippel (1995) states 'debris acts as large roughness elements, reducing average velocity and locally elevating the water surface profile', and some methods can be found in the literature (e.g. Manga & Kirchner 2000; Hygelund & Manga 2003; Bocchiola 2011). This effect was solved here by including drag forces in the governing flow equations as an additional term, similar to roughness, following the methodology proposed by Cea & Vázquez-Cendón (2010). The said authors considered an effective porosity parameter and additional drag to reduce available storage volume due to small-scale obstructions, which are not resolved by the numerical mesh. Of these two terms, which are not present in classic depth-averaged shallow water equations, drag is more relevant, and even more so in the case of logs which affect only part of the depth.

The drag force is therefore included in the flow model as an additional shear stress term in the Saint Venant equations. This shear stress is produced by the drag force of the logs in each finite volume, and is calculated numerically as

$$\tau_{\text{wood},i} = \frac{\sum_{\log s} \mathbf{F}_d}{A_i} \tag{18}$$

$\tau_{\text{wood},i}$ is the shear stress at every finite volume, or mesh element, i, $\mathbf{F}_d$ the drag force vector obtained with Equation (6), and A_i the volume of the 2D finite volume, or area of mesh element, i.

Log interactions

The interactions between the logs and the channel walls or boundaries, and among the logs themselves, have been taken into account in the model by means of changes in log velocity due to contact with the banks or with other pieces, but the effect of branches or roots has been ignored in this work.

If one moving piece of wood meets another piece (floating or resting), the two may collide and continue moving at a different velocity (Figure 1(b)). This new velocity or final

velocity $(\mathbf{v}'_{\log})^i$ of log i is calculated from the initial velocities $(\mathbf{v}_{\log})^{i,j}$ for both colliding pieces i, j as

$$(\mathbf{v}'_{\log})^i = (1+e)\cdot(\mathbf{v}_{\log})^{cm} - e\cdot(\mathbf{v}_{\log})^i \tag{19}$$

where

$$(\mathbf{v}_{\log})^{cm} = \frac{m_i\cdot(\mathbf{v}_{\log})^i + m_j\cdot(\mathbf{v}_{\log})^j}{m_i+m_j} \tag{20}$$

is the velocity of the mass center of the colliding logs, e is the restitution coefficient (equal to 1 assuming elastic interaction) and m_i and m_j are the log masses.

When a piece of wood reaches a bank, it can be entrapped and anchored. In the first case, if the log is anchored (Figure 1(c)), the driving forces decrease due to the reduction of the submerged area, but the resisting forcesare still active around the log, therefore the initial motion condition is re-calculated from these new conditions

$$U^2_{\lim} = \frac{\left((g\cdot\rho_w\cdot L_w\cdot A_w) - \left(g\cdot\rho\cdot A_{\text{sub}}\cdot L_w^{\text{wet}}\right)\right)\cdot(\mu_{\text{bed}}\cdot\cos\alpha - \sin\alpha)}{\left(0.5\cdot C_d\cdot\rho\cdot\left(L_w^{\text{wet}}\cdot h\cdot\sin\theta + A_{\text{sub}}\cdot\cos\theta\right)\right)} \tag{21}$$

where L_w^{wet} is the length of the log inside the river channel.

In the second case, if the log hits a bank or boundary (like in this case a flume wall), the log trajectory and velocity may change to a different pattern. According to our observations during the flume experiments, the log movement after touching the wall is depending on the incidence angle (the angle between the log and the boundary). If this incidence angle is lower than a given value σ_s (a threshold of $\sigma_s = 45^\circ$ is assumed in the simulations, but this value can be modified by the modeler) the movement of the log is treated as sliding or gliding parallel to the wall. On the other hand, if the incidence angle is higher, the log bounces off and changes its trajectory suddenly (Figure 1(d)).

Although this behavior is more complex in real rivers, the developed model used a simplified approach to detect a bouncing or sliding log. To do this, the log end positions are checked at every time step. If a log end is outside the 2D domain, the angle of the log to the wall is used to decide whether it has bounced or slipped against the wall. In both cases, the log is resituated inside the channel as shown in Figure 2. In the case of bouncing, the subsequent movement of the log is towards the center of the channel, perpendicular to the channel wall, and of such a value that the log end remaining outside the channel ends up against the channel wall (Figure 2(a)). In the case of sliding, when a log end is detected to be outside the domain, a rotation is defined with the inside end as the center, and an angle such that the final position of the outside end is on the channel wall (Figure 2(b)). As we have said, the slip angle σ_s must be specified.

Turbulence

Although the flow in river channels is turbulent, for river flows where the geometry is smooth enough and no re-circulation zones appear, roughness acts as the principal factor of vortex stabilization and the inclusion of turbulence models usually has little or no effect on the velocity field (Cea Gómez 2005). Nevertheless, even in these cases it is important to consider turbulence while modeling the transport of suspended substances or sediments, as dispersion is affected by the turbulent viscosity. Similarly, in mountain rivers, small swirls may appear and disappear with an almost chaotic movement, and this turbulence may affect wood transport. 'Iber' includes several turbulence models (constant viscosity coefficient, parabolic, mixing length and k–ε), but when considering the influence of turbulence on wood transport, the Rastogi–Rodi k–ε model (Rastogi & Rodi 1978) has been used, as, of the above, it is the only one that can give information on the magnitude of turbulent kinetic energy.

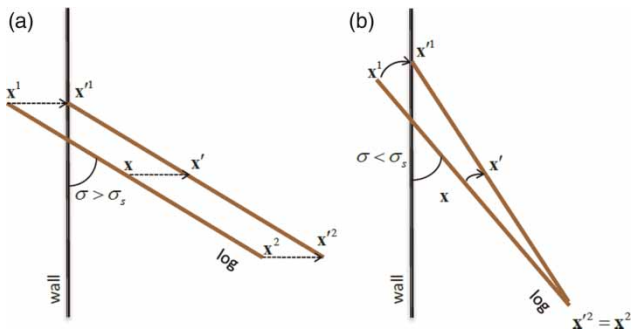

Figure 2 | Recalculation of log position when bouncing (a) or sliding (b) against the channel wall.

For wood transport, the k–ε model has been used to recalculate the flow velocity used to calculate wood velocity. Fluctuations in turbulent velocity can be calculated from the values of turbulent kinetic energy k and a random number λ (Kleinstreuer & Zhang 2003)

$$u' = \lambda\left(\frac{2}{3}k\right)^{1/2} \tag{22}$$

Using this approach, the wood velocity is then calculated using the reconstructed instantaneous water velocity $u = U + u'$, instead of U in Equation (11), which basically means introducing a random component into the motion of logs transported by a turbulent flow. In this way, identical logs dropped into the same spot may end up in different places, differing more the higher the turbulent kinetic energy.

Wood initial and boundary conditions

The numerical model developed needs initial conditions of logs. To do this, the modeler provides initial position of each log (x, y coordinates of mass center and angle with respect to the flow), its length, diameter and wood density for the initial time step.

Inlet boundary conditions (i.e. logs entering the simulation from upstream) can also be assigned to the simulation domain boundaries, specifying a number of wood pieces per minute and its characteristics. Based on our knowledge of the fluvial corridor, riparian vegetation, and wood availability, ranges of maximum and minimum lengths, diameters and density of wood are established. Stochastic variations of these parameters together with position and angle are used to characterize the wood rate entering the model.

EXPERIMENTAL SETUP

Laboratory flume experiments were used for testing and validation of the numerical model. The objective here was to test the accuracy and performance of the numerical model described above. The flume experiences were numerically simulated at scale 1:1.

Description of the experimental setup

Flume experiments were conducted at the Flumen Research Institute laboratories. The flume used is 0.6 m wide and 20 m long, with a horizontal slope and a rectangular cross section with glass sidewalls (see Figure 3), although only the upstream 6 m were used for the experiments. The channel is fed with water from a re-circulatory system. Upstream of the flume there is a triangular sharp-crested weir to control the discharge, and a cobble-filled baffle to dissipate energy and ensure a uniform velocity distribution at the flume entrance. The experiments were designed to validate the numerical model for simple geometries. Further complications with irregular geometries were left for future research.

Round white beech, wooden dowels were used to represent LW pieces in the laboratory. Different scenarios were considered using five sizes of dowels, three different initial dowel densities, three different initial orientations and five different channel geometries. The different

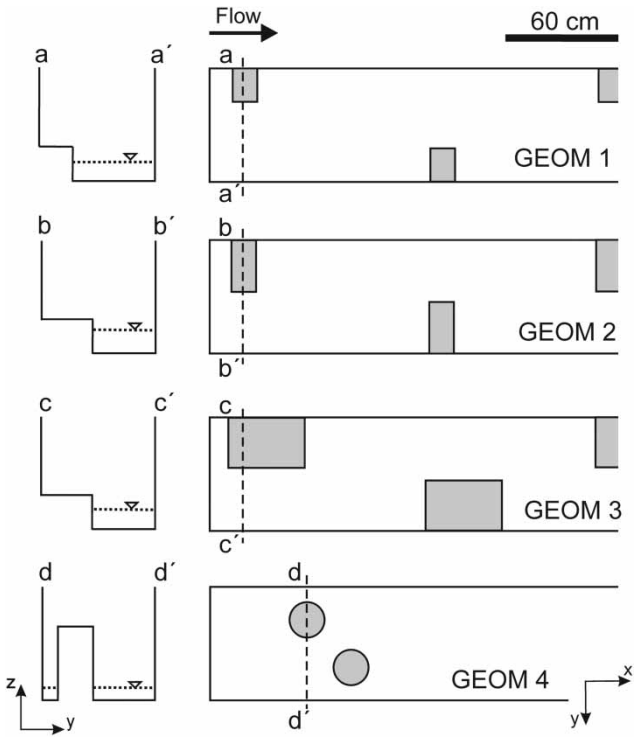

Figure 3 | Flume geometric configurations: longitudinal plans of flume reaches are shown in the right side and cross sections in the left side. Water depth is marked with a dotted line in the cross sections.

experimental scenarios were numerically reproduced and the numerical and experimental results compared.

The five types of pieces used were: (i) type 1: short dowels (0.1 m, less than half the flume width) with medium diameter (10 mm); (ii) type 2: medium dowels (0.2 m, close to half the flume width) with small diameter (8 mm); (iii) type 3: medium dowels (0.2 m, close to half the flume width) with large diameter (12 mm); (iv) type 4: long dowels (0.5 m, more than half the flume width) with medium diameter (10 mm); and (v) type 5: medium dowels (0.2 m) with very large diameter (18 mm). The average density of this type of wood is 720 kg m^{-3}. The logs were painted in bright colors to facilitate monitoring.

The straight geometry of the channel was modified with several lateral alternated constrictions and central obstacles (Figure 3) to form different two-dimensional velocity patterns. Different discharges (12 and 18 L s^{-1}) and boundary conditions (critical depth and weirs of 5.8 and 9.7 cm in height) were combined to achieve low (higher flow velocity) and high water depths (lower flow velocity).

Observation methods

Flow depth and flow velocities were measured on a regular grid, resulting in 40 measured points. The water depth in the flume was measured using a point gauge. The three-dimensional (3D) (u, v, w) velocity field was measured using a Micro Acoustic Doppler Velocimeter (Vectrino, www.nortekusa.com). The sampling volume of the ADV is a 7 mm-long cylinder with 1.8 mm transmit length. The control volume was located 5 cm from the probe to reduce flow interference. The maximum sampling rate of the Vectrino used in the experiments was 200 Hz.

The velocity values resulting from Vectrino measurements are an average of many velocity estimates ('pings'). The uncertainty of each ping is dominated by short-term error, which depends on the size of the transmit pulse and the measurement volume; it is typically a fraction of 1 cm s^{-1} (or ±0.5% of the measured value). The calibration of the velocimeter and data recording was managed using Vectrino Plus software (User Guide 2009) and the raw data obtained was processed and filtered using WinADV software (Wahl 2000).

All flume runs were video recorded using a wide-angle-digital camera installed above the flume to obtain a perpendicular overhead view. The video frames covered the entire flume and were recorded at a rate of 30 frames per second.

The code first extracts the video frames. Each frame is a color image where pixels color is determined by a given combination of red, green and blue intensities ranging between 0 and 255. Figure 4(a) shows the decomposition of one of the video frames into its red, green and blue components. This combination depends on the log color and is chosen so that the log pixels take higher values than the water surface ones in the resulting image. Then, a template of the log length and width is shifted on the just computed channel around the coordinates of the known log center at the preceding frame, using a range of different orientations around the known preceding orientation. These center coordinates and orientation angle are stored and used as initial conditions to search for the log location in the next frame.

Once the log center and orientation have been determined for all video frames, the spatial coordinates of the log center, obtained in image coordinates (i.e. row and column expressed in number of pixels), are transformed into x and y flume coordinates in meter units for their comparison with the numerical results.

EVALUATION OF MODEL PERFORMANCE

For the 2D numerical simulations, computational meshes of quadrilaterals with a side length of 1 cm were used for all channel configurations. For all discharges used, the flow was subcritical throughout the whole domain. Upstream boundary conditions of uniform specific discharge were used for the entire width of the channel. Bed friction is considered using the Manning roughness coefficient, which is assigned to each element of the mesh. Its value is estimated based on the numerical and experimental comparison of steady backwater profiles (0.01 s $m^{-1/3}$) in the same channel but without the constrictions. The simulations were run with and without the k-ε turbulence model.

Hydrodynamic simulations (with no wood transport) succeeded in representing the flow conditions in the flume with good accuracy (numerical and experimental comparison for geometry 1 is shown in Figure 5); the flow velocity has a correlation coefficient of 0.91 ($R^2 = 0.84$). We attribute

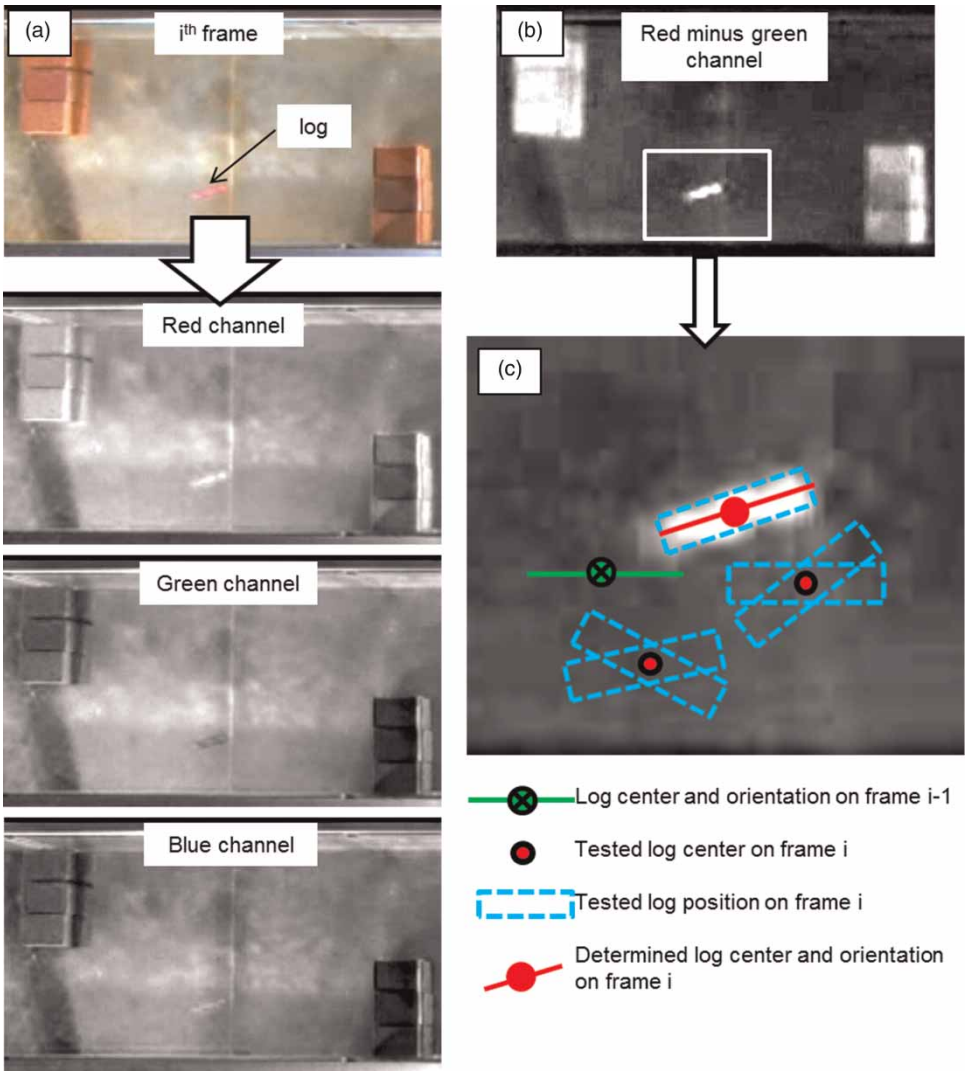

Figure 4 | Computation of the log location on the video frames. (a) Decomposition of the frame into its red, green and blue components. (b) Subtraction of the red and green components on a pixel basis. The pixels gray scale represents red, green and blue intensities ranging between 0 and 255. (c) Some log centers and orientations are tested around the log position in the preceding frame.

deviations mostly to the 3D effect in the flow, which cannot be simulated by the 2D model.

As described above, four different geometries were used to obtain different flow conditions (Table 1).

Log motion

The first verification tests were carried out to check the accuracy of the simulation in describing log motion, including both translation and rotation. Various logs were placed in the flume with different orientations as described above. As expected, logs placed parallel to the flow direction continued to move with this orientation following the maximum velocity line; however, logs initially placed oblique (45°) or perpendicular (90°) to the main flow direction turned until they attained the same orientation as in the previous case (Figure 6).

The same behavior was observed during the flume experiments.

As model results, wood transport can be computed together with common variables such as depth, velocity, Froude number and, if the k–e model is used, turbulent

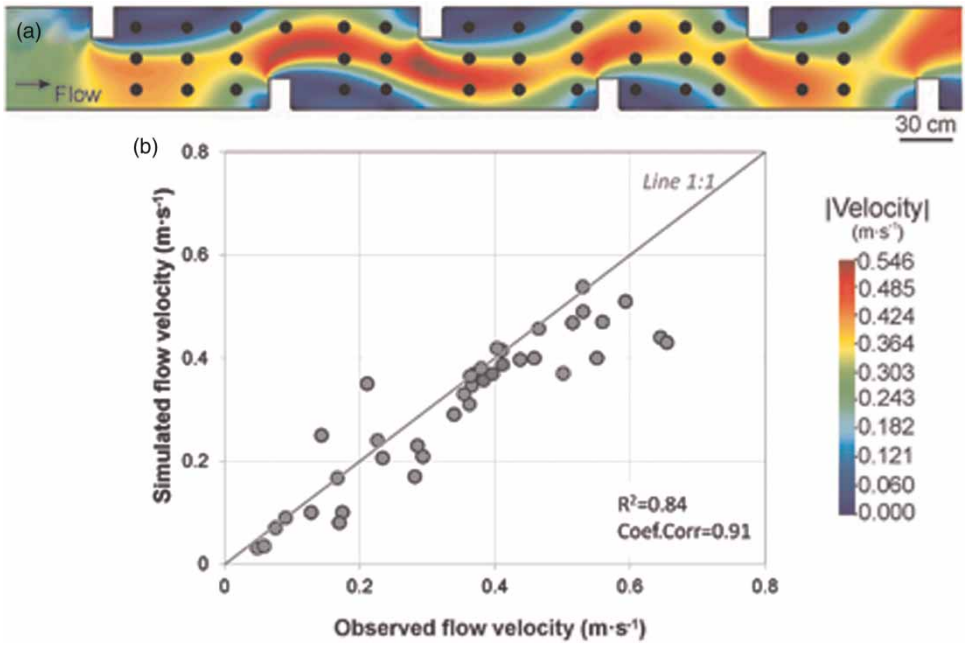

Figure 5 | (a) Measurement points shown over numerical velocity results for geometry 1, with flow from left to right. (b) Velocity values measured and simulated.

Table 1 | Flume test configurations

Geometry	Inlet discharge (L s^{-1})	Outlet boundary condition	Water depth (max-min) (cm)
1. Small lateral constrictions	18	Weir height 5.8 cm	16–10
2. Medium lateral constrictions	18	Weir height 5.8 cm	20–8
3. Large lateral constrictions	12	Weir height 9.7 cm	18–13
4. Two central piers	12	Critical	10–1

viscosity. Figure 7 shows an example of model outputs for simulations of geometry 1 and a single log type 2.

The numerical results for model log positions, trajectories and log velocities were first visually compared with flume records and then used for statistical analysis of their fit with experimental measures. The simulation results were compared with the post-processed video recordings using the correlation coefficient, absolute and squared errors and statistical significance difference (p-value). Figure 8 shows two of these simulations, and their statistics are provided in Table 2.

In general, for all flume geometries no significance differences were found between observed and simulated log position (Figure 9), trajectories and velocities (p-value $<$ 0.05). The correlation coefficient was in all cases $>$0.7, the mean error ranged up to 0.09, and the root mean squared error ranged up to 0.2 m.

Some peculiarities in flow field and log transport were observed due to the various flume geometries and log types analysed (Figure 10).

Flume geometries 1 and 3 present similar water depth conditions although discharge, velocity field and constrictions were different; geometries 2 and 4 present higher water depth variations (difference between inlet or maximum, and outlet or minimum; see Table 1). The highest depth gradient was observed in geometry 2, as well as the largest recirculation areas besides obstacles. Geometry 3 presents the lowest values for flow velocities and geometry 4 the highest. These flow configurations influenced on the log transport. For flume geometries 1 and 3, logs were following the same path (maximum velocity line) with almost no interactions with walls and obstacles or recirculation zones; while for flume geometry 2 logs were more often entering into these eddy areas. This is true for log types 1, 2, 3 and 4; however, we also found differences in log

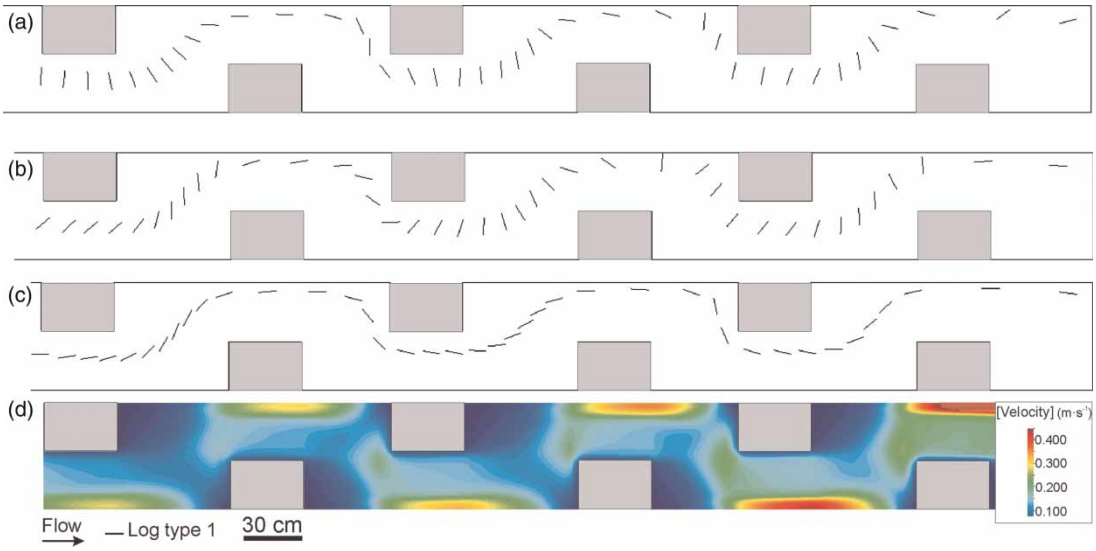

Figure 6 | Results of the numerical model for geometry 3: three logs ((a)–(c)) placed with different orientations (on the left) rotate to a more stable hydrodynamic position, parallel to the flow direction in the maximum velocity line. (d) Module velocity field (m s^{-1}).

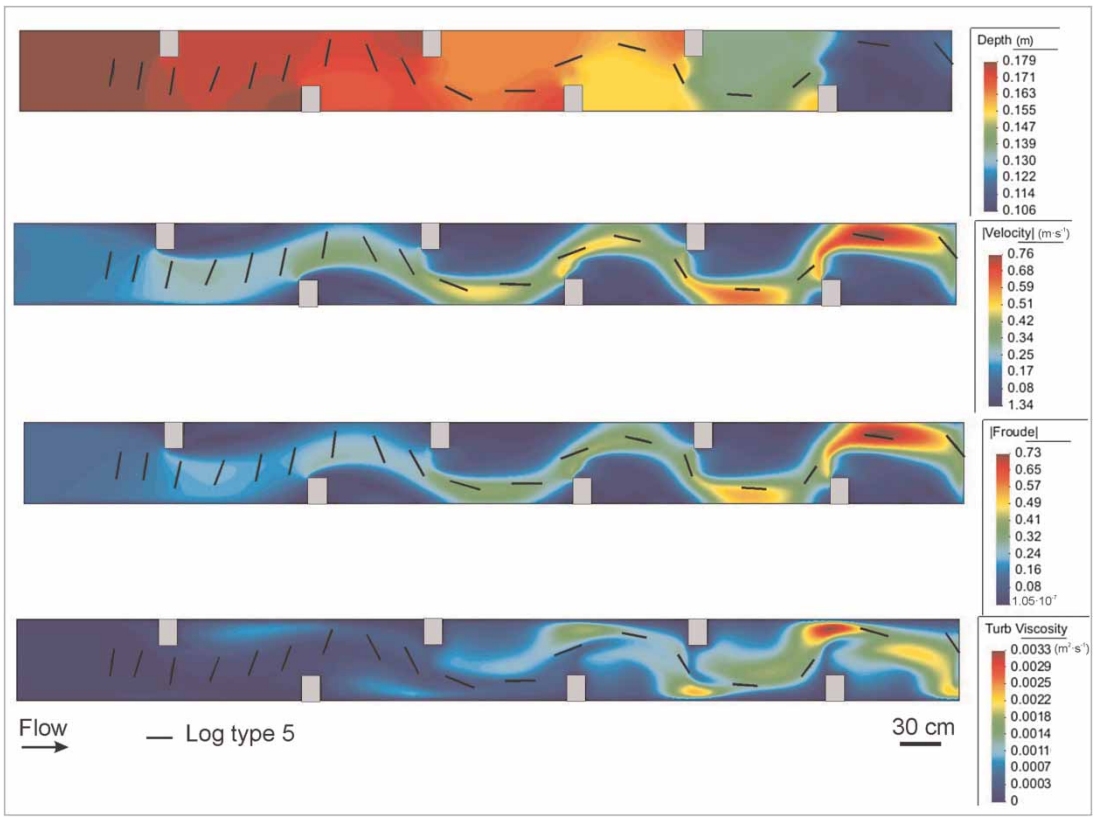

Figure 7 | Model outputs for geometry 1: water depth, flow velocity (module), Froude number and turbulent viscosity are shown together with log trajectory (black lines). Flow direction left to right.

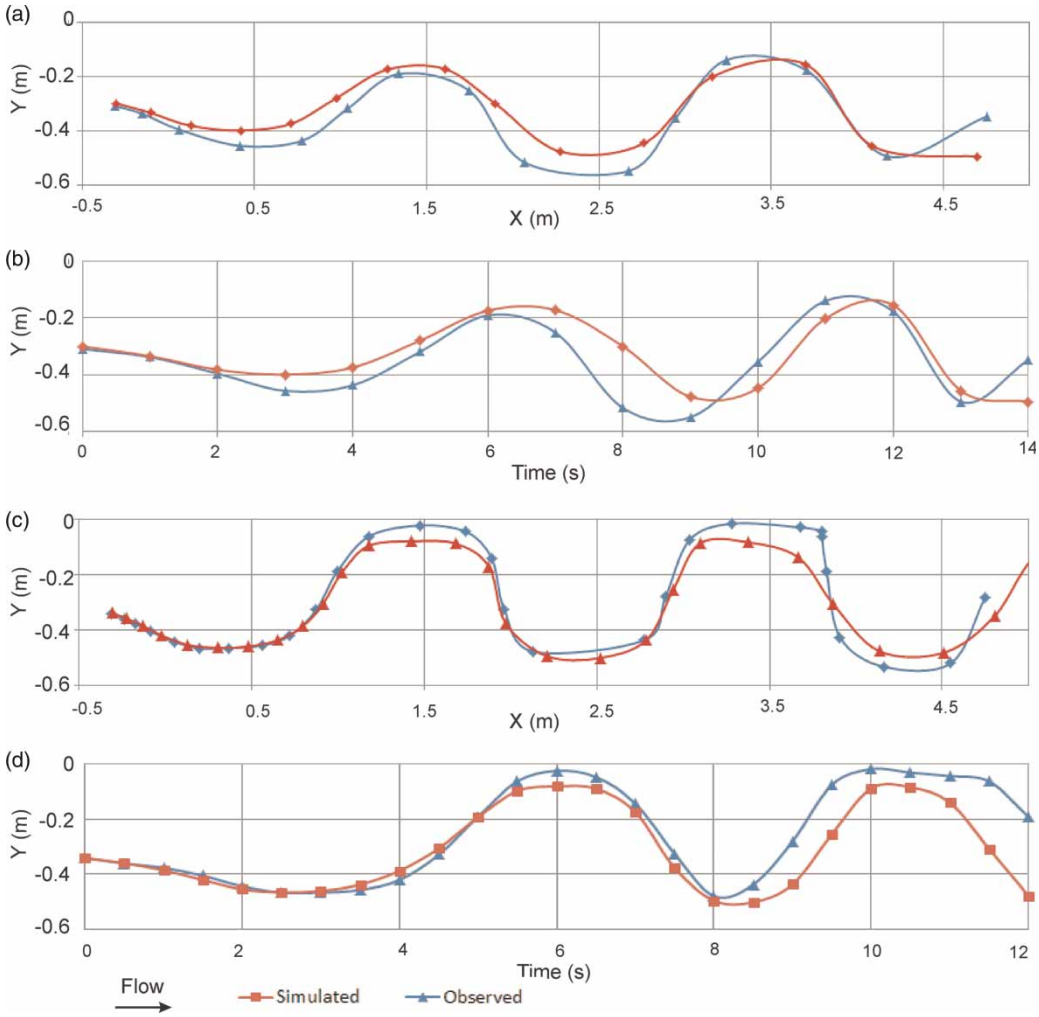

Figure 8 | Observed and simulated log center trajectory and log center position at each time step for geometry 1 ((a) and (b)) and for geometry 2 ((c) and (d)).

Table 2 | Statistics for the test cases shown in Figure 7

	GEOM 1	GEOM 2
p-value (95%IC)	0.002	0.002
MSE (m)	0.019	0.015
RMS	0.096	0.059

motion depending on the log type. Longer logs (logs type 4) were interacting more frequently with the flume walls and obstacles, but the model was able to simulate most of them. On the other hand, shorter pieces (log type 1) were more easily entrapped in recirculation zones behind obstacles, and this was difficult to reproduce perfectly with the model, although it can be simulated. However, the validation in these cases was tricky due to the complex trajectories followed by the logs.

Influence of wood transport on the flow

One significant effect of wood on stream hydrodynamics is the backwater effect due to clogging. Flume configuration 4 allowed us to test this effect.

Log types 1, 2, 3 and 5 were mostly no blockage probability; however, log type 4 showed an approximately 90% blockage probability. Although the flume width is 60 cm and log length 50 cm, the effective width between piers is just 30 cm. When one or more of these long logs is entrapped between the piers, the blockage probability of

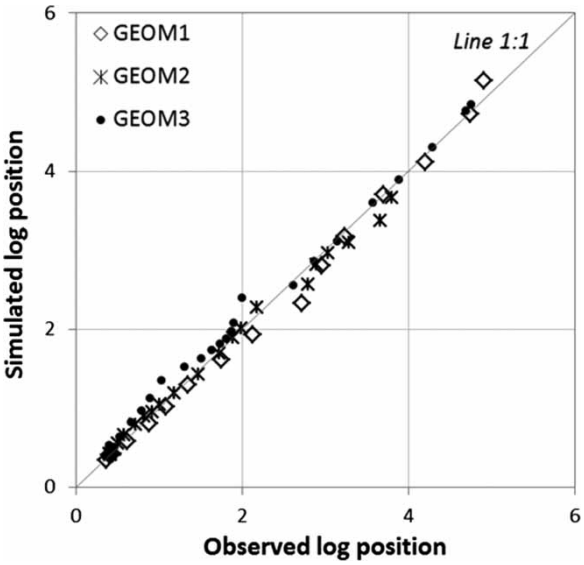

Figure 9 | Observed and simulated log position for geometries 1, 2 and 3.

the other log types increased rapidly. In those cases, log types 2, 3 and 5 were the most easily entrapped.

As Figure 11 shows, the piers blockage due to LW affected water depths, velocities and discharge distribution. The backwater effect caused by the entrapped logs significantly increases water depths (up to 40%) and reduces velocities upstream of the piers (up to 50%). A velocity reduction can also be observed downstream of the pier, caused by the logs traveling at a lower velocity than water due to their interaction with the channel walls.

A 3D effect was observed that could not be reproduced by the model. When logs are clogging the piers some approaching logs were submerged and passed under this woody barrier. Since roots or branches are not present in the used logs, the blockage probability may change for real LW, probably increasing.

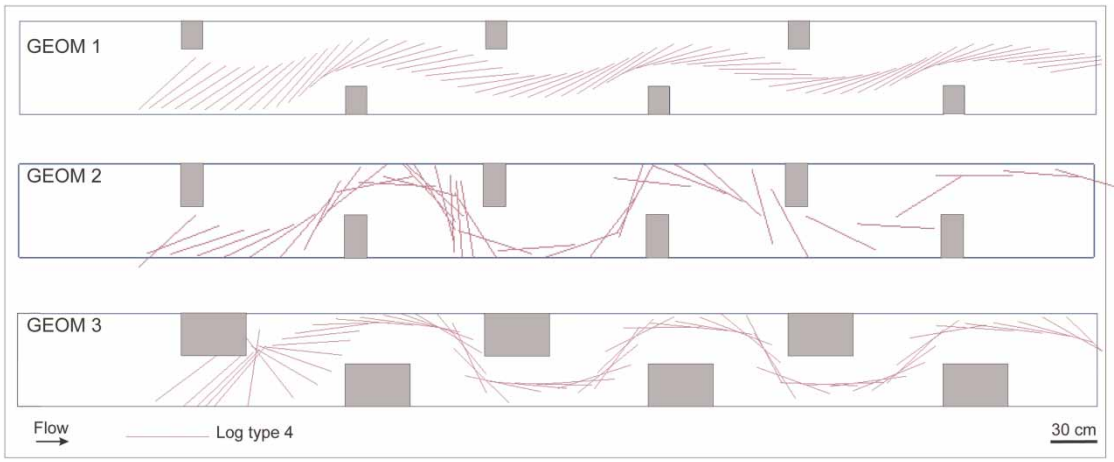

Figure 10 | Numerical results for three geometries (1, 2, 3): a log type 4 is placed in the flume, oblique to the flow and its trajectory change accordingly to the flow conditions.

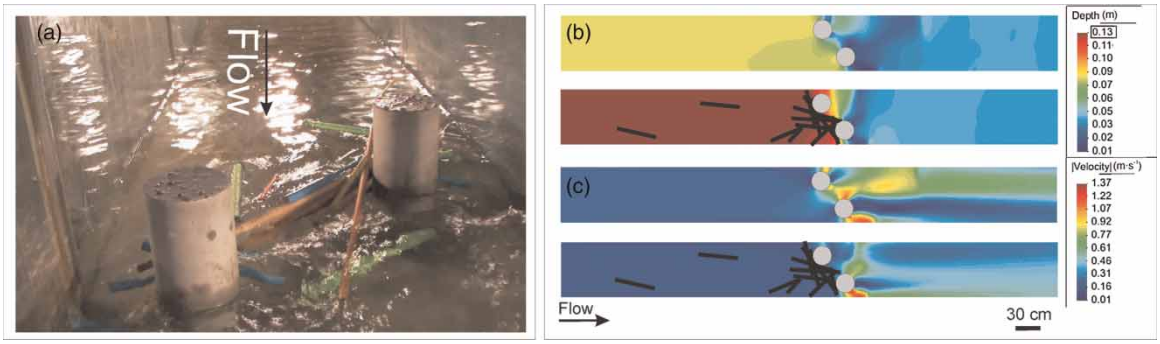

Figure 11 | Numerical results for geometry 4. (a) Flume geometry 4; (b) water depth; (c) velocity field with (black lines) and without LW for a blockage ration of 35% approximately.

Log interactions

The model, as described above, can simulate interactions between logs and the channel configuration and between the logs themselves. Figure 12 shows an example of a log moving in the flow and another log colliding with it; both logs change their trajectory.

If logs show geometries that are more complex (with roots or branches), some other interactions can happen, or interacted logs can continue moving together after collision. The model is not able to simulate these effects so far.

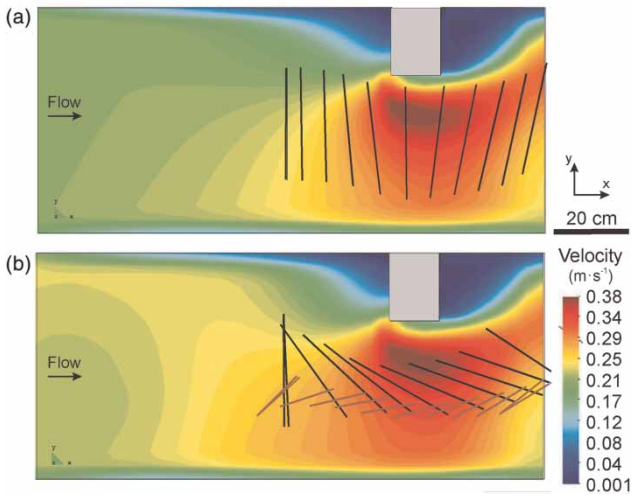

Figure 12 | Numerical model results of log interaction: (a) a log is moving and rotating according to the velocity field; (b) a second log collides with log 1 and changes its trajectory. Flow direction left to right.

Effect of the turbulence model

When the k–ε model is not used, the simulated flow patterns change, and the flume flow is represented less precisely. We see that if the turbulence model is not used, the velocity is higher and logs therefore move faster, increasing the error in log position with respect to the observations (Figure 13).

As explained above, log velocity is calculated from the flow velocity and the transport inhibition parameter. Wood and flow velocities are very similar (correlation coefficient >0.8) but not equal (Figure 14). This slight difference is due to the instantaneous velocity reconstruction from the turbulence model. If no turbulence model is used, log velocity and flow velocity are exactly equal, except in the case of logs interacting with each other or with the channel walls.

DISCUSSION

An existing 2D hydrodynamic numerical model has been modified to simulate wood transport. The model has been tested and validated using flume experiments. There follows below a description of the limitations of the method, enhancements with respect to previous works, the main challenges encountered when developing the method and potential uses and applications.

Model implications and limitations

The numerical model developed to simulate the transport of wood together with hydrodynamics represents a potential

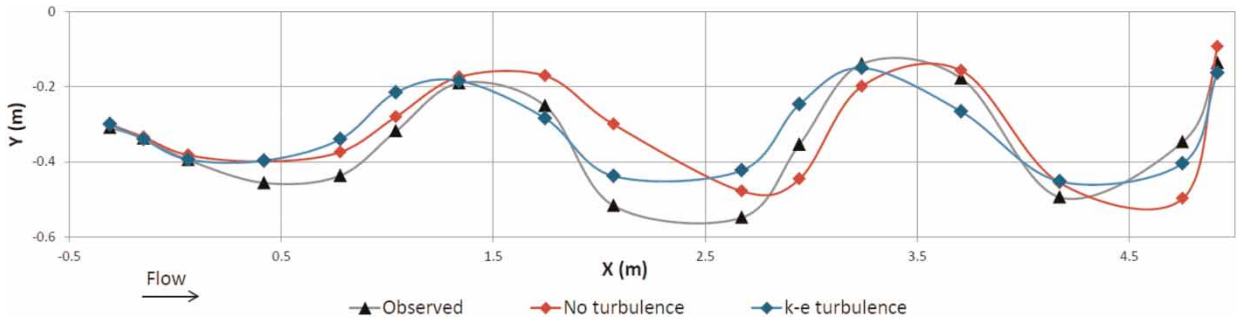

Figure 13 | Observed and simulated (with and without turbulence) log center trajectories for geometry 3.

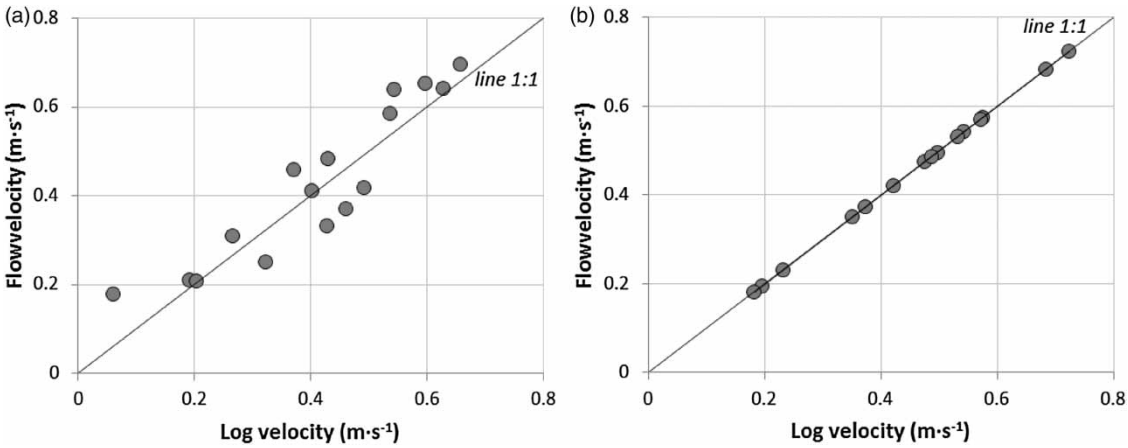

Figure 14 | Flow and log velocities computed for simulation solving turbulence (a) and simulation with no turbulence model applied (b).

tool for predicting and simulating wood transport and its influence on hydrodynamics. Model validation highlights its viability, although as usual in modeling approaches, some simplifications are assumed.

In the words of Malamud & Baas (2013), it is generally better to have a model with fewer parameters if increased understanding is not gained by the addition of more parameters. Following these thoughts and the concept of model parsimony defined by Gernert (2007) we decided to keep the model as simple as possible in order to better validate the results with the flume experiments.

Most previous research on log motion uses simplified continuity or Manning equations to estimate flow velocity (Braudrick & Grant 2000, Braudrick *et al.* 2001; Bocchiola *et al.* 2008, Bocchiola 2011) or measure reach-average velocity using salt dilution methods (Wilcox & Wohl 2006). Some others have used 1D or 2D models (Merten *et al.* 2010; Mazzorana *et al.* 2011a, b, 2013), but first computing the hydraulics and then using the results to calculate wood mobilization. Here, we developed a numerical model, which calculates the two horizontal components of log velocity at each time step at each end of every log and at the log center at the same time as the flow velocity.

Flume experiments have been used here to test and validate the correct performance of the numerical model. Therefore, the first challenge was to accurately reproduce the hydrodynamics of the flume, as the geometries used produced a recirculating flow with an important 2D component. Although the hydraulic model was calibrated, deviations were observed between the simulations and the experience. These deviations conditioned the reproduction of log transport. In general, for all flume geometries and log types, no significance differences were found between observed and simulated log position, trajectories and velocities (p-value <0.05). The correlation coefficient was in all cases >0.7.

There are several reasons for these differences between the observations and the simulations. One is that a two-dimensional model cannot reproduce the 3D effects. Another reason is that when collecting data with the Vectrino, the equipment has to be submerged a few centimeters in the flow and the near-surface velocity fields (responsible for the wood velocities and trajectories) could not be measured. The highest differences were observed near the flume outlet, where there was a sharp-crested weir. This lower accuracy could be due to the 3D effects that can occur near the weir wall. The third reason can be related to the post process of the videos. The used code detects the log and computes its center, and orientation on each frame. Once the log center has been determined, the spatial image coordinates are transformed into x and y flume coordinates. Some bias can be related to this latter process.

However, despite these deviations a good correlation was found for all geometries (correlation coefficient >0.8).

Wood motion is also affected by flow turbulence. The developed method is able to incorporate this effect into the simulations to some degree. When turbulence is computed, the model recalculates instantaneous log velocity using the instantaneous flow velocity reconstructed from the computed

kinetic energy, as explained above under 'Turbulence'. The results also showed that turbulence might change due to the presence of logs; therefore, in the authors' opinion this is an important contribution to hydrodynamic simulation.

Application of the model to real rivers

'Iber' is a two-dimensional model for simulating turbulent-free surface unsteady flow and environmental processes in river hydraulics. Since this model has a friendly interface which facilitates its application (Corestein *et al.* 2010; Bladé *et al.* 2012), the application of the new module ('Woody Iber') in real rivers or streams is straightforward.

For verification of the numerical modeling, a real scale model of the experimental facility was used. Nevertheless, if the experiments were to be extrapolated to a real stream using, for example, a geometric scale of 20, the flume would represent a physical model of a reach 12 m wide and 100 m long, the prototype discharge would be around 32 $m^3 s^{-1}$, with maximum prototype velocities around 3 m s^{-1}, and prototype logs ranging from 2 to 10 m in length and from 0.2 to 0.36 m in diameter, which are values that could be encountered in real streams.

Probably one of the most relevant steps when applying the method in rivers is to establish wood initial and boundary conditions. An in-depth understanding of the fluvial corridor and the riparian vegetation is needed to establish the availability of wood and ranges for its maximum and minimum lengths, diameters and density. Methodologies have been developed previously for characterizing wood, its distribution along the river and potential availability, and its recruitment processes (see Abbe & Montgomery 2003; Andreoli *et al.* 2007; Mazzorana *et al.* 2009; Wohl & Jaeger 2009; Wohl *et al.* 2011). However, here the number of input trees (logs) has to be estimated, and logs have to be characterized individually. This can be approached using the forest inventory and with the help of geographic information systems (Rigon *et al.* 2012), as well as by applying fuzzy-logic principles (Ruiz-Villanueva *et al.* 2014).

The first application of this model in a real case is described in Ruiz-Villanueva *et al.* (2013). In this work, a bridge clogging process due to LW transport during a flash flood event was reproduced by modeling individual wood pieces moving in the flow. A combination of internal weir and gate conditions was used to represent the bridge geometry, and the model simulated how the wood interacts with the bridge affect hydrodynamics. The establishment of different scenarios for the wood transport allowed us to study the influence of the inlet boundary conditions on the bridge clogging. In addition, the model succeeded in predicting the deposition patterns of wood along the reach, showing the places prone to top form woody jams, validated by direct observations in the field.

Potential applications

Flood inundation modeling is one of the most common applications of depth-averaged shallow water models and this may be the main direct application of the method presented in this paper. In relation to flood hazard analysis, the main problem is the clogging of critical sections such as bridges. The simulation of LW transport at critical stream geometry configurations may therefore be of interest. In terms of drift entrainment and transport, the effects of blockage due to LW accumulations at river bridges may be studied from a perspective of either flood hazard (backwater effects; see Mazzorana *et al.* 2011a, b, 2013) or infrastructure evaluation (failure, pier scour, or sizing; see Schmocker & Hager 2010, 2011).

From another point of view, the ecological importance of LW is reflected in areas where there is decreased flow velocity and increased flow depth, where habitat suitability for fish species colonization is enhanced (Bocchiola 2011), so log deposition areas could be an ecological indicator. LW has also become a central theme in river management and restoration (Benda & Sias 2003).

As mentioned above, the method presented here can be implemented in any two-dimensional hydrodynamic model provided it uses an explicit scheme, and thus a small time step. At present, a wide range of commercial and non-commercial modeling tools are available based on FVM or FEM that satisfy this requirement.

CONCLUSIONS

The main goal of the present model was to simulate the transport of LW in streams, accounting for the mutual

interaction between wood and river hydrodynamics. A numerical model was coupled to 2D hydraulic software. Flume experiments were used in a straight channel with obstructions to validate the model's capacity to accurately reproduce the movement of floating logs under different hydraulic conditions at relatively short timescales. The good agreement between the numerical model and prototype-scale simulations of log transport in a flume substantiates the validity of the proposed approach.

Although notable simplifications were adopted for the development of the presented tool and further work is needed to better simulate the complexity of wood transport in natural watercourses, this model constitutes at present a first attempt to incorporate wood transport in two-dimensional hydrodynamic simulation. Our efforts are motivated at least in part by a desire to improve scientific understanding of wood dynamics in rivers; this numerical model primarily was intended to allow realistic virtual simulations, not only in the laboratory but also in real rivers. Further research will allow the model to be improved and tested in different environments and for different purposes, as we think this can be a useful tool in the field of fluvial geomorphology and related branches.

ACKNOWLEDGEMENTS

This work was funded by the MAS Dendro-Avenidas project (CGL2010-19274), of the Spanish National Research Plan, and by the Geological Survey of Spain. The lead author acknowledges the grant obtained from the Spanish Ministry of Science and Innovation for a 3-month research period at the Flumen Research Institute (UPC). The authors are grateful to Georgina Corestein and Hans Sánchez for their help with programming, Soledad Estrella for her help with the laboratory experiments, Ceferino Robledo for recording the flume experiments and Joaquim Rabada for his help with IT.

REFERENCES

Abbe, T. & Montgomery, R. 2003 Patterns and processes of wood debris accumulation in the Queets river basin, Washington. *Geomorphology* **51**, 81–107.

Allen, J. B. & Smith, D. L. 2012 Characterizing the impact of geometric simplification on large woody debris using CFD. *Int. J. Hydr. Eng.* **1**, 1–14.

Andreoli, A., Comiti, F. & Lenzi, M. A. 2007 Characteristics, distribution and geomorphic role of large woody debris in a mountain stream of the Chilean Andes. *Earth Surf. Proc. Land.* **1692**, 1675–1692.

Benda, L. E. & Sias, J. C. 2003 A quantitative framework for evaluating the mass balance of in-stream organic debris. *Forest Ecol. Manag.* **172**, 1–16.

Bladé, E., Cea, L., Corestein, G., Escolano, E., Puertas, J., Vázquez-Cendón, M. E., Dolz, J. & Coll, A. 2012 *Iber* – Herramienta de simulación numérica del flujo en ríos. *Rev. Int. Metod. Numer.* **30** (1), 1–10.

Bocchiola, D. 2011 Hydraulic characteristics and habitat suitability in presence of woody debris: A flume experiment. *Adv. Water Resour.* **34**, 1304–1319.

Bocchiola, D., Catalano, F., Menduni, G. & Passoni, G. 2002 An analytical–numerical approach to the hydraulics of floating debris in river channels. *J. Hydrol.* **269**, 65–78.

Bocchiola, D., Rulli, M. C. & Rosso, R. 2006 Flume experiments on wood entrainment in rivers. *Adv. Water Resour.* **29**, 1182–1195.

Bocchiola, D., Rulli, M. C. & Rosso, R. 2008 A flume experiment on the formation of wood jams in rivers. *Water Resour.* **44**, 1–17.

Braudrick, C. & Grant, G. E. 2000 When do logs move in rivers? *Water Resour. Res.* **36**, 571–583.

Braudrick, C. A., Grant, G. E., Ishikawa, Y. & Ikeda, H. 1997 Dynamics of wood transport in streams: a flume experiment. *Earth Surf. Proc. Land.* **22**, 669–683.

Braudrick, C. A., Grant, G. E., Northwest, P. & Forest, U. S. 2001 Transport and deposition of large woody debris in streams: a flume experiment. *Geomorphology* **41**, 263–283.

Brooks, A. P., Abbe, T., Cohen, T., Marsh, N., Mika, S., Boulton, A., Broderick, T., Borg, D. & Rutherfurd, I. 2006*Design Guidelines for the Reintroduction of Wood into Australian Streams*. Land & Water, Canberra, Australia.

Buxton, T. H. 2010 Modeling entrainment of waterlogged large wood in stream channels. *Water Resour. Res.* **46**, W10537.

Cea Gómez, L. 2005 An unstructured finite volume model for unsteady turbulent shallow water flow with wet-dry fronts: Numerical solver and experimental validation. PhD Dissertation. *Universidad de A Coruña Departamento de Métodos Matemáticos y de Representación Programa de doctorado en Ingeniería Civil*, Galicia, Spain.

Cea, L. & Vázquez-Cendón, M. E. 2010 Unstructured finite volume discretization of two-dimensional depth-averaged shallow water equations with porosity. *Int. J. Numer. Meth. Fluids.* **63**, 903–930.

Collins, B. D., Montgomery, D. R., Fetherston, K. L. & Abbe, T. B. 2012 The floodplain large-wood cycle hypothesis: a mechanism for the physical and biotic structuring of temperate forested alluvial valleys in the North Pacific coastal ecoregion. *Geomorphology* **139–140**, 460–470.

Comiti, F., Andreoli, A., Lenzi, M. & Mao, L. 2006 Spatial density and characteristics of woody debris in five mountain rivers of the Dolomites (Italian Alps). *Geomorphology* **78**, 44–63.

Comiti, F., Andreoli, A., Mao, L. & Lenzi, M. A. 2008a Wood storage in three mountain streams of the Southern Andes and its hydro-morphological effects. *Earth Surf. Proc. Land.* **33**, 242–262.

Comiti, F., Mao, L., Preciso, E., Picco, L., Marchi, L. & Borga, M. 2008b Large wood and flash floods: evidences from the 2007 event in the Davca basin (Slovenia). (D. Wrachien, C. A. Brebbia & M. A. Lenzi, eds) *Monitoring, Simulation, Prevention and Remediation of Dense and Debris Flow II*, 60, WIT Press, UK, pp. 173–182.

Comiti, F., Agostino, V. D., Moser, M., Lenzi, M. A., Bettella, F., Agnese, A. D., Rigon, E., Gius, S. & Mazzorana, B. 2012 Preventing wood-related hazards in mountain basins: from wood load estimation to designing retention structures. In: *12th Congress INTERPRAEVENT 2012 – Grenoble/France Conference Proceedings*, pp. 651–662.

Corestein, G., Bladé, E., Cea, L., Lara, Á. & Escolano, E. 2010 Iber, a river dynamics simulation tool. In: *Proceedings of GiD conference: GiD 2010*, CIMNE.

Curran, J. C. 2010 Mobility of large woody debris (LW) jams in a low gradient channel. *Geomorphology* **116**, 320–329.

DHI 2007 MIKE 21 and MIKE FLOOD User and Reference Manuals. DHI Software, DHI Water and Environment, Denmark.

Gernert, D. 2007 Ockham's razor and its improper use. *J. Sci. Exp.* **21**, 135–140.

Gippel, C. J. 1995 Environmental hydraulics of large woody debris in streams and rivers. *J. Environ. Eng.* **121**, 388.

Gurnell, A. M., Pie, H. & Northwest, P. 2002 Large wood and fluvial processes. *Freshwater Biol.* **47**, 601–619.

Gutierrez-Andres, J., Lhomme, J., Weisberger, A., Cooper, A. & Gouldby, B. 2008 Testing and application of a practical new 2D hydrodynamic model. (P. Samuels, S. Huntington, W. Allsop & J. Harrop, eds) *Flood Risk Management: Research and Practice*. Taylor & Francis, London.

Haga, H., Kumagai, T., Otsuki, K. & Ogawa, S. 2002 Transport and retention of coarse woody debris in mountain streams: An *in situ* field experiment of log transport and a field survey of coarse woody debris distribution. *Water Resour. Res.* **38**, 1126.

Hupp, C. R. & Bornette, G. 2003 Vegetation and fluvial processes and forms in temperate areas. In: *Tools in Fluvial Geomorphology* (G. M. Kondolf & H. Piégay, eds). John Wiley & Sons, Chichester, pp. 269–288.

Hygelund, B. & Manga, M. 2003 Field measurements of drag coefficients for model large woody debris. *Geomorphology* **51**, 175–185.

Jackson, C. R. & Sturm, C. A. 2002 Woody debris and channel morphology in first- and second-order forested channels in Washington's coast ranges. *Water Resour. Res.* **38** (9), 1177–1190.

Kasprak, A., Magilligan, F. J., Nislow, K. H. & Snyder, N. P. 2011 A LIDAR derived evaluation of watershed scale large woody debris sources and recruitment mechanisms: coastal Maine, USA. *River Res. Appl.* **28**, 1462–1476.

Kleinstreuer, C. & Zhang, Z. 2003 Laminar-to-turbulent fluid-particle flows in a human airway model. *Int. J. Multiphase Flow* **29**, 271–289.

Langford, T. E. L., Langford, J. & Hawkins, S. J. 2012 Conflicting effects of woody debris on stream fish populations: implications for management. *Freshwater Biol.* **57**, 1096–1111.

Lassettre, N. S. & Kondolf, G. M. 2012 Large woody debris in urban stream channels: redefining the problem. *River Res. Appl.* **28**, 1477–1487.

LeVeque, R. J. 2002 *Finite Volume Methods for Hyperbolic Problems*. Cambridge University Press, Cambridge.

MacFarlane, W. A. & Wohl, E. 2003 Influence of step composition on step geometry and flow resistance in step-pool streams of the Washington Cascades. *Water Resour. Res.* **39**, 1037.

MacVicar, B. & Piégay, H. 2012 Implementation and validation of video monitoring for wood budgeting in a wandering piedmont river, the Ain River (France). *Earth Surf. Proc. Land.* **37**, 1272–1289.

Macvicar, B. J., Henderson, A., Comiti, F., Oberlin, C. & Pecorari, E. 2009 Quantifying the temporal dynamics of wood in large rivers: field trials of wood surveying, dating, tracking, and monitoring techniques. *Earth Surf. Proc. Land.* **34**, 2031–2046.

Magilligan, F., Nislow, K., Fisher, G., Wright, J., Mackey, G. & Laser, M. 2008 The geomorphic function and characteristics of large woody debris in low gradient rivers, coastal Maine, USA. *Geomorphology* **97**, 467–482.

Malamud, B. D. & Baas, A. C. W. 2013 Nine considerations for constructing and running geomorphological models. In: *Treatise on Geomorphology* (J. Shroder & A. C. W. Baas (Editor in Chief), eds). Academic Press, San Diego, CA, vol. 2, Quantitative Modeling of Geomorphology, pp. 6–28.

Manga, M. & Kirchner, J. W. 2000 Stress partitioning in streams by large woody debris. *Water Resour. Res.* **36**, 2373–2379.

Manners, R. B., Doyle, M. W. & Small, M. J. 2007 Structure and hydraulics of natural woody debris jams. *Water Resour. Res.* **43**, 1–17.

Martin, D. J. & Benda, L. E. 2001 Patterns of instream wood recruitment and transport at the watershed scale. *Trans. Am. Fish. Soc.* **130**, 940–958.

May, C. L. & Gresswell, R. E. 2003 Large wood recruitment and redistribution in headwater streams in the southern Oregon Coast Range, U.S.A. *Can. J. Forest. Res.* **33**, 1352.

Mazzorana, B., Zischg, A., Largiader, A. & Hübl, J. 2009 Hazard index maps for woody material recruitment and transport in alpine catchments. *Hazards Earth Syst. Sci.***9**, 197–209.

Mazzorana, B., Comiti, B. & Fuchs, S. 2013 A structured approach to enhance flood hazard assessment in mountain streams. *Nat. Hazards* **67**, 991–1009.

Mazzorana, B., Hübl, J., Zischg, A. M. & Largiader, A. 2011a Modelling woody material transport and deposition in alpine rivers. *Nat. Hazards* **56**, 425–449.

Mazzorana, B., Comiti, F., Volcan, C. & Scherer, C. 2011b Determining flood hazard patterns through a combined stochastic–deterministic approach. *Nat. Hazards* **59**, 301–316.

Merten, E., Finlay, J., Johnson, L., Newman, R., Stefan, H. & Vondracek, B. 2010 Factors influencing wood mobilization in streams. *Water Resour. Res.* **46**, 1–13.

Montgomery, D. 2003 Wood in rivers: interactions with channel morphology and processes. *Geomorphology* **51**, 1–5.

Montgomery, D. R. & Piégay, H. 2003 Wood in rivers: interactions with channel morphology and processes. *Geomorphology* **51**, 1–5.

Moulin, B. & Piégay, H. 2004 Characteristics and temporal variability of large woody debris trapped in a reservoir on the River Rhone (Rhone): implications for river basin management. *River Res. App.* **20**, 79–97.

Moulin, B., Schenk, E. R. & Hupp, C. R. 2011 Distribution and characterization of in-channel large wood in relation to geomorphic patterns on a low-gradient river. *Earth Surf. Proc. Land.* **36**, 1137–1151.

Murillo, J., Rodríguez-Pallares, M., Andrés-Urrutia, A., Brufau, P. & García-Navarro, P. 2008 A mathematical model for numerical simulation of shallow water flow: Description and practical application of GUAD 2D, Proc. of the iEMSs 2008. *Int. Env. Mod. Soft. Soc.* **3**, 1431–1438.

Rigon, E., Comiti, F. & Lenzi, M. A. 2012 Large wood storage in streams of the Eastern Italian Alps and the relevance of hillslope processes. *Water Resour. Res.* **48**, W01518.

Rastogi, A. & Rodi, W. 1978 Predictions of heat and mass transfer in open channels. *J. Hydr. Eng. Div.* **104**, 397–420.

Ruiz-Villanueva, V., Bladé-Castellet, E., Díez-Herrero, A., Bodoque, J. M. & Sánchez-Juny, M. 2013 Two-dimensional modelling of large wood transport during flash floods. *Earth Surf. Process. Landforms*. doi: 10.1002/esp.3456.

Ruiz-Villanueva, V., Díez-Herrero, A., Ballesteros, J. A. & Bodoque, J. M. 2014 Potential large woody debris recruitment due to landslides, bank erosion and floods in mountain basins: a quantitative estimation approach. *River Res. Applic.* **30**, 81–97.

Schmocker, L. & Hager, W. H. 2010 Drift accumulation at River Bridges. In: *River Flow 2010* (A. Dittrich, K. Koll, J. Aberle & P. Geisenhainer, eds). Bundesanstalt für Wasserbau.

Schmocker, L. & Hager, W. H. 2011 Probability of drift blockage at bridge decks. *J. Hydraul. Eng.* **137**, 480–492.

Seo, J. I. & Nakamura, F. 2009 Scale-dependent controls upon the fluvial export of large wood from river catchments. *Rivers* **80**, 786–800.

Swanson, F. J. 2003 Wood in Rivers: a landscape perspective. *Am. Fish. Soc. Symp.* **37**, 299–313.

Thevenet, A., Citterio, A. & Piégay, H. 1998 A new methodology for the assessment of large woody debris accumulations on highly modified rivers (example of two French Piedmont rivers). *Regul. River* **14**, 467–483.

Vázquez-Cendón, M. E. 1999 Improved treatment of source terms in upwind schemes for the shallow water equations in channels with irregular geometry. *J. Comput. Phys.* **148**, 497–526.

Versteeg, H. K. & Malalasekera, W. 2007 *An Introduction to Computational Fluid Dynamics: The Finite Volume Method*, 2nd edn. Pearson Education, Harlow.

Wahl, T. L. 2000 Analyzing ADV Data Using WinADV. *2000 Joint Conference on Water Resources Engineering and Water Resources Planning & Management*, July 30–August 2, 2000, Minneapolis, Minnesota.

Wallerstein, N. P., Alonso, C. V., Bennett, S. J. & Thorne, C. R. 2001 Distorted Froude-scaled flume analysis of large woody debris. *Earth Surf. Proc. Land.* **26**, 1265–1283.

Webb, A. A. & Erskine, W. D. 2003 A practical scientific approach to riparian vegetation rehabilitation in Australia. *J. Environ. Manage.* **68**, 329–341.

Wilcox, A. C. & Wohl, E. 2006 Flow resistance dynamics in step-pool stream channels: 1. Large woody debris and controls on total resistance. *Water Resour. Res.* **42**, 1–16.

Wilcox, A. C., Peckarsky, B. L., Taylor, B. W. & Encalada, A. C. 2008 Hydraulic and geomorphic effects on mayfly drift in high-gradient streams at moderate discharges. *Ecohydrology* **186**, 176–186.

Wohl, E. 2011 Threshold-induced complex behavior of wood in mountain streams. *Geology* **39**, 587–590.

Wohl, E. & Jaeger, K. 2009 A conceptual model for the longitudinal distribution of wood in mountain streams. *Earth Surf. Proc. Land.* **34**, 329–344.

Wohl, E., Bolton, S., Cadol, D., Comiti, F., Goode, J. R. & Mao, L. 2011 A two end-member model of wood dynamics in headwater neotropical rivers. *J. Hydrol.* **462–463**, 1–10.

First received 28 February 2013; accepted in revised form 6 February 2014. Available online 12 March 2014